Microscopic in-medium nucleon-nucleon cross sections with improved Pauli blocking effects

B. Chen,[1] F. Sammarruca,[1] and C. A. Bertulani[2]
[1]*Physics Department, University of Idaho, Moscow, Idaho 83844-0903, USA*
[2]*Department of Physics and Astronomy, Texas A&M University-Commerce, Commerce, Texas 75428, USA*
(Received 21 April 2013; published 23 May 2013)

We present updated predictions of effective elastic nucleon-nucleon cross sections intended for use in nucleus-nucleus reactions. A novel characteristic of the present approach combines all microscopic medium effects included in the Dirac-Brueckner-Hartree-Fock G-matrix with a Pauli blocking mechanism which is more appropriate for applications in ion-ion reaction models as compared to a previous approach. The effective in-medium cross section is found to be quite sensitive to the description of Pauli blocking in the final configurations.

DOI: 10.1103/PhysRevC.87.054616 PACS number(s): 21.30.Fe, 21.65.−f

I. INTRODUCTION

The investigation of the effective nucleon-nucleon (NN) interaction in dense hadronic matter is a topic of fundamental importance for nuclear reactions at intermediate energies ($20 \lesssim E_{\rm lab} \lesssim 300$ MeV/nucleon) and for nuclear structure in general. The relevant literature is very vast. Reference [1] is just a representative example of the traditional microscopic approach where two-nucleon correlations in nuclear systems are introduced through the G-matrix. Moreover, the effective NN interaction is the main ingredient of microscopic predictions of the nuclear equation of state (EOS) and thus impacts the properties of compact stars. Dense hadronic matter can also be created in the laboratory in energetic heavy-ion (HI) collisions. Simulations of HI collisions are typically based on transport equations and describe the evolution of a nonequilibrium system of strongly interacting hadrons undergoing two-body collisions in the presence of a mean field. The Boltzmann-Uehling-Uhlenbeck equation [2,3] and quantum molecular dynamics [4], along with their relativistic counterparts [5–7], have been typically employed to describe intermediate-energy HI reactions. *In-medium* two-body cross sections are therefore an important component of such simulations.

In direct reactions at intermediate energies the NN cross sections are often used as input to obtain quantum refractive and diffractive effects, replacing the role of optical potentials commonly used in low energy reactions [8]. Examples such as knockout (stripping and diffraction dissociation) reactions, elastic scattering, charge exchange, and excitation of giant resonances are often carried out using reaction mechanisms based on the construction of scattering matrices built from the underlying NN scattering. Reaction calculations at intermediate to high energy are often conducted within the framework of the Glauber approximation [9] and have been a frequent tool for testing nuclear models and constraining nuclear sizes. In fact, the description of complex nuclear reactions at intermediate energies based on individual NN collisions has a long tradition. In the framework of the Glauber model, the reaction cross section is written in terms of the "thickness function," which is the product of the averaged NN cross section and the overlap integral of the target and projectile local densities.

In-medium NN cross sections have been calculated with a variety of methods. In semiphenomenological approaches, one makes the assumption that the transition matrix in the medium is approximately the same as the one in vacuum and that medium effects come in only through the use of effective masses in the phase-space factor [10–12]. Then, the in-medium cross section is scaled (relative to its value in vacuum) as the square of the ratio of the (reduced) masses. Phenomenological formulas, such as the one in Ref. [13], have been developed for practical purposes and combine the energy dependence of empirical free-space NN cross sections with the density dependence of some microscopic models.

Microscopic predictions based on a medium-modified collision matrix were reported, for instance, in Ref. [14], where Dirac-Brueckner-Hartree-Fock (DBHF) medium effects were applied to obtain a medium-modified K-matrix, and in Ref. [15], where the predictions are based on the Brueckner-Hartree-Fock scheme together with the Paris potential. More recent microscopic calculations applied DBHF medium effects to produce a complex G-matrix including consideration of isospin dependence in asymmetric nuclear matter [16].

It is the purpose of this paper to present our updated predictions of microscopic in-medium elastic NN cross sections with an improved description of Pauli blocking. The main objective is to produce two-body cross sections which include, microscopically, all important medium effects and are suitable for realistic applications in nucleus-nucleus scattering at intermediate energies including direct and central collisions. As explained in Sec. II, we start from a one-boson-exchange NN potential, which describes well the elastic part of the NN interaction up to high energy. Thus, as long as we are not interested in pion production, which is negligible up to, at least, several hundreds of MeV, it is reasonable to use NN elastic cross sections as input to the reaction model. Of course, the elastic part of the NN interaction can and does generate inelastic nucleus-nucleus scattering.

In Sec. II, we describe the details of the calculation and highlight the differences with our previous approach. We then present a selection of results (Sec. III) followed by our conclusions and outlook (Sec. IV).

II. DESCRIPTION OF THE CALCULATION

A. The Dirac-Brueckner-Hartree-Fock *G*-matrix

The starting point of our calculation is a realistic NN interaction which is applied in the nuclear medium without any additional free parameters. We use relativistic meson theory, which we find to be an appropriate framework to deal with the high momenta encountered in dense matter. In particular, the one-boson-exchange (OBE) model has proven very successful in describing NN data in free space and has a good theoretical foundation.

The OBE potential is defined as a sum of one-particle-exchange amplitudes of certain bosons with given mass and coupling. In general, six non-strange bosons with masses below 1 GeV/c^2 are used. Thus,

$$V = \sum_{\alpha=\pi,\eta,\rho,\omega,\delta,\sigma} V_\alpha^{\mathrm{OBE}}, \tag{1}$$

with π and η pseudoscalar, σ and δ scalar, and ρ and ω vector particles. For more details, see Ref. [17]. Among the many available OBE potentials, some being part of the "high-precision generation" [18,19], we seek a momentum-space potential developed within a relativistic scattering equation, such as the one obtained through the Thompson [20] three-dimensional reduction of the Bethe-Salpeter equation [21].

First, a self-consistent calculation of (symmetric or asymmetric) nuclear matter is performed within the DBHF approach [22]. This step yields, along with the EOS, the self-consistent nuclear matter potential, which is conveniently parametrized in terms of nucleon effective masses (see Ref. [22] for details). Then, the Thompson equation is solved for two nucleons scattering at some positive energy in the presence of a mean field due to the medium. The presence of the medium is accounted for through the (previously calculated) effective masses (applied in the two-nucleon propagator and also in the Dirac spinors representing the nucleons, consistent with the DBHF philosophy) and the presence of the (angle-averaged) Pauli operator to account for Pauli blocking of the *intermediate states*.

In the usual free-space scattering scenario, the two-body cross section is typically represented as a function of the incident laboratory energy, uniquely related to the nucleon momentum in the two-body center-of-mass frame, $\mathbf{q}$, through relativistic invariants which yield the well-known relation $E_{\mathrm{lab}} = 2q^2/m$. In nuclear matter, though, the Pauli operator depends also on the total momentum of the two nucleons in the nuclear matter rest frame. For simplicity, in the past we have used in-vacuum kinematics to define the total momentum of the two-nucleon system (that is, we assumed that the target nucleon is at rest, on the average). Schematically, the effect of the Pauli principle on intermediate states arises in the G-matrix through the in-medium scattering equation [23]:

$$\langle \mathbf{q}|\mathrm{G}(\mathbf{p})|\mathbf{q}_0\rangle = \langle \mathbf{q}|\mathrm{V}|\mathbf{q}_0\rangle - \int \frac{d^3q'}{(2\pi)^3} \times \frac{\langle \mathbf{q}|\mathrm{V}|\mathbf{q}'\rangle\, Q(\mathbf{q}',\mathbf{p})\langle \mathbf{q}'|\mathrm{G}(\mathbf{p})|\mathbf{q}_0\rangle}{E(\mathbf{p},\mathbf{q}') - E_0 - i\epsilon}, \tag{2}$$

with $\mathbf{q}_0$, $\mathbf{q}$, and $\mathbf{q}'$ the initial, final, and intermediate relative momenta of the NN pair in their center of mass, and $\mathbf{p}$ their total momentum. E is the energy of the two-nucleon system in the center-of-mass, and E_0 is the same quantity on-shell.

The medium effects we include in the G-matrix are Pauli blocking of the intermediate (virtual) states via the angle-averaged Pauli operator; modification of the single-particle energies to include the presence of the nuclear matter potential; and density-dependent nucleon spinors in the OBE potential through the use of nucleon effective masses. The first two effects are typically applied in all conventional Brueckner-Hartree-Fock calculations, whereas the third one is characteristic of the Dirac-Brueckner approach.

To account for Pauli blocking of the *final state*, we define the total elastic cross section as

$$\bar{\sigma}_{NN}(q) = \int \left(\frac{d\sigma}{d\Omega}\right)^{\mathrm{DBHF}} Q(q,\, p,\, \theta,\, \rho)\, d\Omega, \tag{3}$$

where $(d\sigma/d\Omega)^{\mathrm{DBHF}}$ is the elastic differential cross section obtained from the G-matrix amplitudes as described above. θ is the scattering angle and k_F the Fermi momentum. The presence of the Pauli operator in Eq. (3) signifies that the integration domain is restricted by [16]

$$\frac{k_F^2 - p^2 - q^2}{2pq} \leqslant \cos\,\theta \leqslant \frac{p^2 + q^2 - k_F^2}{2pq}. \tag{4}$$

Setting $Q = 1$ in Eq. (3) amounts to ignoring Pauli blocking of the final state. [The virtual intermediate states are always subjected to Pauli blocking during the G-matrix calculation which produces the amplitudes contained in $(d\sigma/d\Omega)^{\mathrm{DBHF}}$.] Additional simplifications result from the assumption that the differential cross section is isotropic.

B. The average in-medium cross section and Pauli blocking effects

The cross section defined in Eq. (3) refers to an idealized scenario where a projectile nucleon, with some momentum above the bottom of the Fermi sea, strikes a target nucleon while both embedded in an infinite medium. For application to a realistic nucleus-nucleus scattering scenario, it is best to consider the situation depicted in Fig. 1, where the two Fermi spheres represent the local densities of the target and projectile ions. $\mathbf{k}$ is the incident momentum (the momentum of the colliding *nuclei* relative to each other), whereas $\mathbf{k_1}$ and $\mathbf{k_2}$ are the momenta of any two *nucleons*. That is, $\mathbf{k_1}$ and $\mathbf{k_2} + \mathbf{k}$ are the momenta of the two nucleons with respect to the same point. Then, the relative momentum $2\mathbf{q}$ and the total momentum $2\mathbf{p}$ are given by $2\mathbf{q} = \mathbf{k}_2 + \mathbf{k} - \mathbf{k}_1$, and $2\mathbf{p} = \mathbf{k}_1 + \mathbf{k}_2 + \mathbf{k}$, respectively. The larger circle in the figure is centered at $\mathbf{p}$ while $|\mathbf{q}|$ is the radius of the scattering sphere. The vector $2\mathbf{q}$ can rotate around the scattering sphere while maintaining constant magnitude due to energy-momentum conservation.

Notice that, with the definitions given above, relative momenta which are off the symmetry axis of the two Fermi spheres (the $\mathbf{k}$ direction) are allowed, which is not the case with the assumptions made in Eq. (3). That is, the two interacting nucleons can have momenta in arbitrary directions. In turn, this

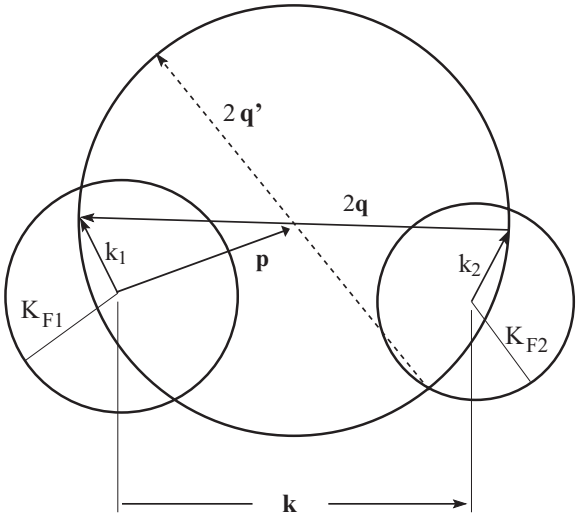

FIG. 1. Geometrical representation of Pauli blocking.

impacts the solid angle allowed by Pauli blocking, as shown below. (For completeness, we provide a detailed derivation of the allowed solid angle in the next subsection.)

In preparation for the nucleus-nucleus calculation, it is shown in Refs. [24,25] that the *average* NN cross section (assuming isotropy of the NN differential cross section) can be written as

$$\bar{\sigma}_{NN}(k) = \frac{1}{V_{F1}V_{F2}} \int d\mathbf{k}_1 d\mathbf{k}_2 \frac{2q}{k} \sigma_{NN}(q) \int_{\text{Pauli}} d\Omega, \quad (5)$$

where k_1 and k_2 are smaller than k_{F1} and k_{F2}, respectively, and the angular integrations extend over all possible directions of $\mathbf{k_1}$ and $\mathbf{k_2}$ allowed by Pauli blocking. Often, the empirical free-space NN cross section is used in the integral. In our case, $\sigma_{NN}(q) = \sigma^{\text{DBHF}}(q)$ is the (microscopic) NN cross section which contains additional medium effects as described in the previous section. V_{F1} and V_{F2} are the volumes of the two (in general different) Fermi spheres. Because of azimuthal asymmetry, Eq. (5) can be reduced to a fivefold integration. Notice that the "symmetric" choice $\mathbf{q} = \mathbf{p} = \mathbf{k}/2$ [26] amounts to making the approximations we adopted when writing Eq. (3).

Finally, for an actual nucleus-nucleus scattering with given E/A, the average cross section given above becomes a function of the laboratory energy $E(k)$ and the local densities of the colliding nuclei, $\rho_i = 2k_{Fi}^3/(3\pi^2)$, and are ready to be used in typical high-energy calculations. This is usually done by defining the average nucleon-nucleon cross section at the distance of closest approach $\mathbf{b}$ between the projectile and the target as

$$\langle \sigma_{NN}(E,b) \rangle = \frac{\int d^3r_1 \, \rho_1(\mathbf{r}_1)\rho_2(\mathbf{r}_1+\mathbf{b}) \, \sigma_{NN}(E,\rho_1,\rho_2)}{\int d^3r_1 \rho_1(\mathbf{r}_1)\rho_2(\mathbf{r}_1+\mathbf{b})}, \quad (6)$$

where ρ_i is the local density (at point $\mathbf{r}$) inside nucleus i and $\sigma_{NN}(E,\rho_1,\rho_2)$ is the in-medium NN cross section.

The calculation of reaction cross sections in high-energy collisions is best described in the eikonal formalism. The "survival amplitudes" (or S matrices) in the eikonal approximation

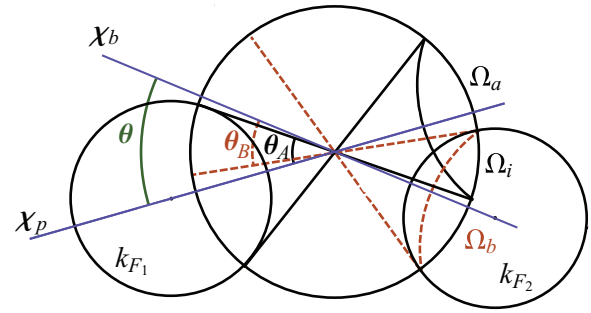

FIG. 2. (Color online) Two-dimensional projection of the geometry of Pauli blocking.

are given by [9,24]

$$S(E,b) = \exp\left[-\frac{\langle \sigma_{NN}(E,b)\rangle}{4\pi} \int_0^\infty dq \, q \, \rho_1(q)\rho_2(q) J_0(qb)\right], \quad (7)$$

where $\rho_{1,2}(q)$ is the Fourier transform of the nuclear densities of the projectile and target, and the reaction cross sections are

$$\sigma_R = 2\pi \int db \, b[1 - |S(b)|^2]. \quad (8)$$

Applications to stable and unstable nuclei using Eqs. (6)–(8) and our new prescription of Pauli blocking effects will be the subject of a future work.

C. Derivation of the Pauli-allowed solid angle

As mentioned in the previous section, the relative momentum $2\mathbf{q}$ and the total momentum $2\mathbf{p}$ are given as $2\mathbf{q} = \mathbf{k_2} + \mathbf{k} - \mathbf{k_1}$, and $2\mathbf{p} = \mathbf{k_1} + \mathbf{k_2} + \mathbf{k}$. We also define a vector $2\mathbf{b}$ as $2\mathbf{b} = \mathbf{k_2} + \mathbf{k_1} - \mathbf{k}$. Assuming that the collision is elastic, conservation of energy and momentum requires

$$2\mathbf{p} = \mathbf{k_1'} + \mathbf{k_2'} + \mathbf{k}, \quad 2\mathbf{q'} = \mathbf{k_2'} - \mathbf{k_1'} + \mathbf{k}, \quad 2\mathbf{b} = \mathbf{k_1'} + \mathbf{k_2'} - \mathbf{k}. \quad (9)$$

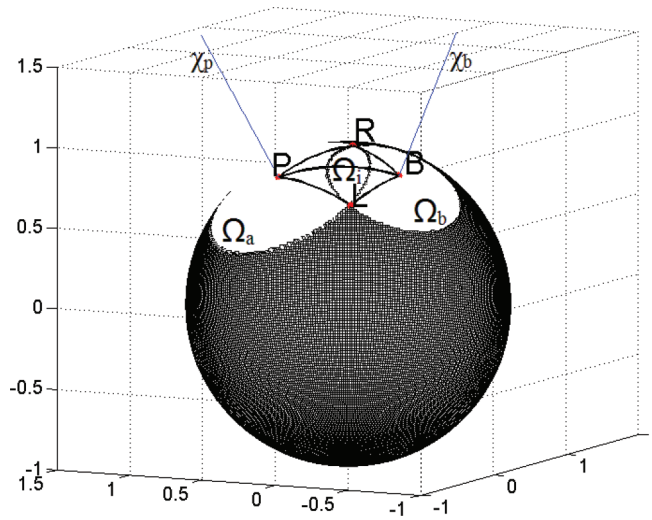

FIG. 3. (Color online) Pauli blocking of two nucleons in three dimensions.

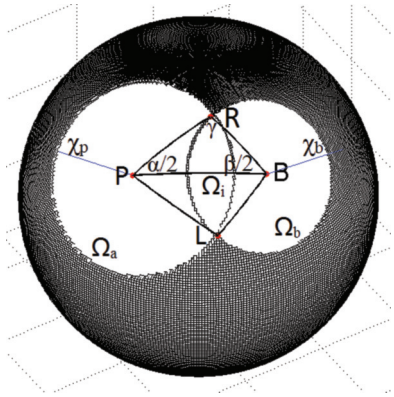

FIG. 4. (Color online) A different view of Pauli blocking of two nucleons in three dimensions.

The quantities $\mathbf{k}_1'$ and $\mathbf{k}_2'$ are the momenta of two nucleons after the collision, whereas $\mathbf{q}'$ is the relative momentum after collision, with $|\mathbf{q}'| = |\mathbf{q}|$. Because of the Pauli exclusion principle, the following restrictions apply:

$$|\mathbf{k}_1'| = |\mathbf{p} - \mathbf{q}'| > k_{F1}, \quad |\mathbf{k}_2'| = |\mathbf{b} + \mathbf{q}'| > k_{F2}, \tag{10}$$

or

$$\begin{aligned} p^2 + q^2 - 2pq\cos\alpha_1 &> k_{F1}^2, \\ b^2 + q^2 + 2bq\cos\alpha_2 &> k_{F2}^2. \end{aligned} \tag{11}$$

In the equations above, α_1 is the angle between $\mathbf{p}$ and $\mathbf{q}'$, and α_2 the angle between $\mathbf{b}$ and $\mathbf{q}'$. As illustrated in Fig. 2, we have

$$\cos\theta_A = \frac{p^2 + q^2 - k_{F1}^2}{2pq}, \quad \cos\theta_B = \frac{b^2 + q^2 - k_{F2}^2}{2bq}, \tag{12}$$

with θ_A and θ_B the excluded polar angles. The excluded solid angles for each nucleon are then given by

$$\Omega_a = 2\pi(1 - \cos\theta_A), \qquad \Omega_b = 2\pi(1 - \cos\theta_B), \tag{13}$$

and therefore the total allowed solid angle can be obtained from

$$\Omega_{\text{Pauli}} = 4\pi - 2(\Omega_a + \Omega_b - \bar{\Omega}), \tag{14}$$

where $\bar{\Omega}$ represents the intersection of the two conical sections Ω_a and Ω_b. The full calculation has already been done in Ref. [25]; however, in this paper we will use a slightly different approach to calculate $\bar{\Omega}$. Figure 3 shows how Ω_a and Ω_b are projected on the surface of a unit sphere. If Ω_i is the intersection of Ω_a and Ω_b, it is obvious that

$$\Omega_i = \begin{cases} 0 & \text{if } \theta > \theta_A + \theta_B; \\ \Omega_b & \text{if } \theta_B < \theta_A,\ \theta < |\theta_B - \theta_A|; \\ \Omega_a & \text{if } \theta_A < \theta_B, \theta < |\theta_B - \theta_A|. \end{cases} \tag{15}$$

The case $|\theta_B - \theta_A| < \theta < \theta_A + \theta_B$ is more complex than the other three cases and a more detailed study is needed. As shown in Fig. 4, P and B are the centers of the two circular projections Ω_a and Ω_b. The two circular contours intersect at R and L. $\alpha/2$, $\beta/2$, and γ are the internal angles of the spherical triangle PRB. The circular sectors of Ω_a and Ω_b have areas equal to $\alpha\Omega_a/(2\pi)$ and $\beta\Omega_b/(2\pi)$, respectively. The intersection area of Ω_a and Ω_b is given by

$$\Omega_i = \frac{\alpha}{2\pi}\Omega_a + \frac{\beta}{2\pi}\Omega_b - 2\Delta_{PRB}. \tag{16}$$

Here, Δ_{PRB} is the area of the spherical triangle PRB. To obtain an expression for $\alpha/2$, first we define the center of the unit sphere, O, as the origin of the system, and χ_p along the z axis. Point B is at location $(1, \theta, \alpha/2)$, while point L has coordinates $(1, \theta_A, 0)$. We can then write

$$\mathbf{OB} \cdot \mathbf{OL} = \cos\theta_B = \cos\theta_A\cos\theta + \sin\theta_A\sin\theta\cos(\alpha/2), \tag{17}$$

from which $\alpha/2$ can be readily obtained as

$$\alpha/2 = \arccos\left(\frac{\cos\theta_B - \cos\theta\cos\theta_A}{\sin\theta\sin\theta_A}\right). \tag{18}$$

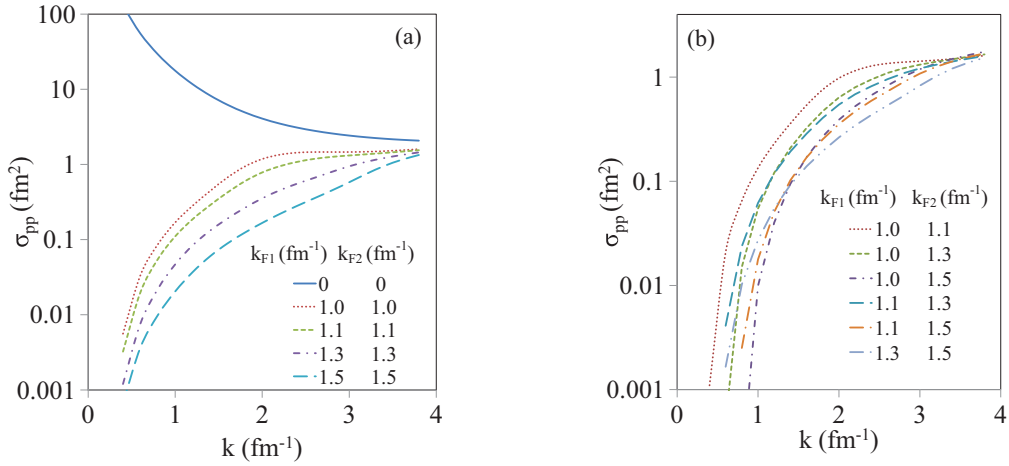

FIG. 5. (Color online) In-medium pp cross section calculated as in Eq. (5) for a variety of (a) symmetric ($k_{F1} = k_{F2}$) and (b) asymmetric ($k_{F1} \neq k_{F2}$) situations.

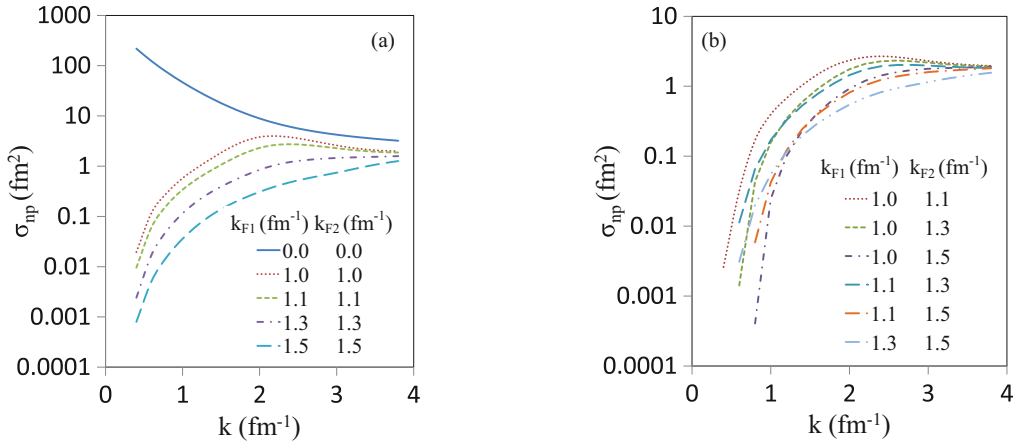

FIG. 6. (Color online) As in Fig. 5, but for np scattering.

In a similar fashion we find $\beta/2$ to be given by

$$\beta/2 = \arccos\left(\frac{\cos\theta_A - \cos\theta\cos\theta_B}{\sin\theta\sin\theta_B}\right). \tag{19}$$

Applying the law of cosines of spherical trigonometry,

$$\cos\gamma = -\cos(\alpha/2)\cos(\beta/2) + \sin(\alpha/2)\sin(\beta/2)\cos\theta, \tag{20}$$

we obtain

$$\gamma = \arccos[-\cos(\alpha/2)\cos(\beta/2) + \sin(\alpha/2)\sin(\beta/2)\cos\theta]. \tag{21}$$

From Girard's theorem of spherical trigonometry, we have

$$\Delta_{PRB} = \alpha/2 + \beta/2 + \gamma - \pi. \tag{22}$$

Inserting Eqs. (21) and (22) into Eq. (16), the solid angle Ω_i is found to have the following value:

$$\Omega_i = 2\{\pi - \cos\theta_A\cos^{-1}(\delta_{AB}) - \cos\theta_B\cos^{-1}(\delta_{BA}) - \cos^{-1}\left[\cos\theta\sqrt{(1-\delta_{AB}^2)(1-\delta_{BA}^2)} - \delta_{AB}\delta_{BA}\right]\}, \tag{23}$$

where

$$\delta_{ij} = \frac{\cos\theta_i - \cos\theta\cos\theta_j}{\sin\theta\sin\theta_j}. \tag{24}$$

Noticing that while $\theta + \theta_A + \theta_B > \pi$, Ω_a and Ω_b have two intersections on the hemisphere, we have

$$\bar{\Omega} = \Omega_i(\theta, \theta_A, \theta_B) + \Omega_i(\pi - \theta, \theta_A, \theta_B). \tag{25}$$

III. RESULTS

A. Effective NN cross sections

We begin by showing in Fig. 5 the average in-medium pp cross section calculated as in Eq. (5). On the left, we display a variety of cases with equal Fermi momenta, whereas asymmetric cases are shown on the right. Figure 6 contains the same information for the np cross section. After "overcoming" complete Pauli blocking, the cross section generally rises with increasing incident momentum. In the np case, we observe, at least at the lower densities, a tendency to reach a broad maximum. In all cases, the cross sections become nearly flat

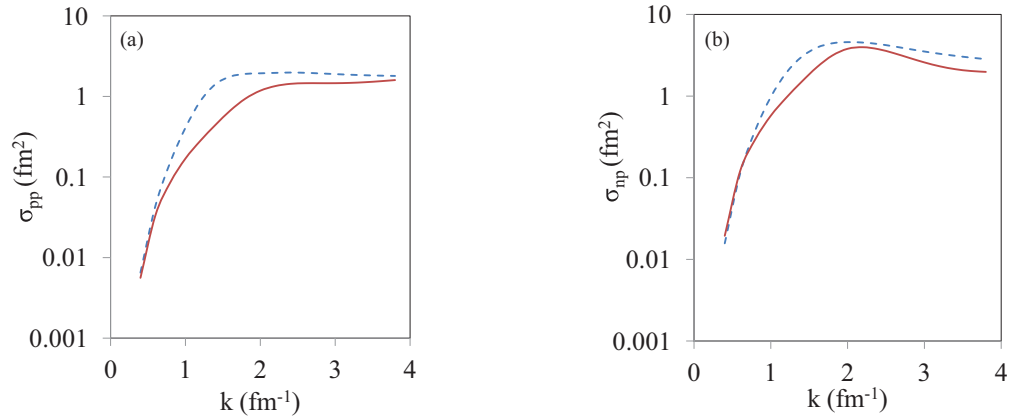

FIG. 7. (Color online) (a) pp and (b) np in-medium cross sections calculated from Eq. (5) with $k_{F1} = k_{F2} = 1.0$ fm^{-1}. Solid red: predictions as in Figs. 5 and 6; dashed blue: the input NN cross section is evaluated in free space. See text for details.

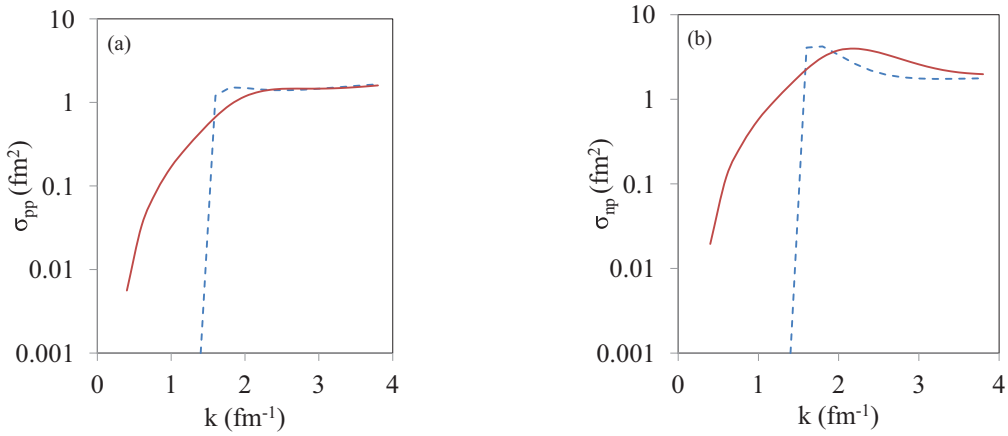

FIG. 8. (Color online) (a) pp and (b) np in-medium cross sections with $k_{F1} = k_{F2} = 1.0$ fm^{-1}. Solid red: predictions as in Figs. 5 and 6; dashed blue: predictions obtained with Eq. (3).

at the larger momenta and begin to approach the free-space predictions.

Figures 5 and 6 are more insightful when compared with Fig. 7. There, the pp and np cross sections shown by the dashed blue line are also calculated with Eq. (5), but the input NN cross sections in the integrand are evaluated in free space. Thus, comparing the two curves on the left-hand side (or on the right for np) shows the impact of the additional medium effects [besides those coming from the $\int_{\text{Pauli}} d\Omega$ factor in Eq. (5)] originating from the G-matrix calculation and included in σ_{NN} in the case of the solid curves. (These effects were described in Sec. II A.) The impact is noticeable, with the microscopic medium effects further suppressing the cross section and shifting the position of the peak. We have chosen a particular case ($k_{F1} = k_{F2} = 1.0$ fm^{-1}) for the purpose of demonstration, but the trend is similar for other densities.

Figure 8 is crucial for the point that we wish to make. There, for pp and np (on the left and right, respectively), we compare the cross sections calculated from Eq. (5) to the corresponding ones evaluated with Eq. (3) instead. The predictions from Eq. (3) have a sharper rise from zero and a more pronounced peak structure. As is reasonable, differences are large at low momenta, where the scattering is most sensitive to the description of Pauli blocking, particularly near the onset of the cross section. Again, we have taken a representative case, but this pattern is common to all densities. It will be interesting to explore the impact of such differences on reaction cross sections, our next objective.

IV. CONCLUSIONS

Pauli blocking is perhaps the most important mechanism impacting the collision of two fermions in the medium. It is known to have a substantial effect on the scattering probability, that is, the in-medium cross section. In this paper, we predict in-medium effective NN cross sections suitable for applications to nucleus-nucleus scattering. The microscopic NN elastic cross sections, modified by all medium effects implied by the Dirac-Brueckner-Hartree-Fock theory of nuclear matter, are properly averaged so as to account for all possible directions of the relative momentum of two nucleons in the two colliding Fermi spheres. The more realistic description of the collision geometry amounts to an improved description of Pauli blocking as compared to a previous approach [16]. We find the effective NN cross sections to be very sensitive to the description of the Pauli blocking geometry.

Our future plans include the application of these cross sections in Glauber reaction calculations with stable and unstable nuclei. In closing, we also note that in-medium cross sections are related to the mean-free path of a nucleon, a fundamental quantity in the description of nucleon propagation in nuclear matter.

ACKNOWLEDGMENTS

Support from the US Department of Energy under Grants No. DE-FG02-03ER41270, No. DE-FG02-08ER41533, and No. DE-FG02-10ER41706 is acknowledged.

[1] H. Müther and A. Polls, Prog. Part. Nucl. Phys. **45**, 243 (2000).
[2] G. F. Bertsch and S. Das Gupta, Phys. Rep. **160**, 189 (1988).
[3] W. Cassing, W. Metag, U. Mosel, and K. Niita, Phys. Rep. **188**, 363 (1990).
[4] J. Aichelin, Phys. Rep. **202**, 235 (1991).
[5] C. M. Ko, Q. Li, and R. C. Wang, Phys. Rev. Lett. **59**, 1084 (1987).
[6] B. Blättel, V. Koch, W. Cassing, and U. Mosel, Phys. Rev. C **38**, 1767 (1988).
[7] H. Sorge, H. Stöcker, and W. Greiner, Ann. Phys. (NY) **192**, 266 (1989).
[8] C. A. Bertulani and P. Danielewicz, *Introduction to Nuclear Reactions* (IOP, London, 2004).
[9] R. J. Glauber, *Lectures on Theoretical Physics*, Vol. I (Interscience, New York, 1959).
[10] V. R. Pandharipande and S. C. Pieper, Phys. Rev. C **45**, 791 (1992).
[11] D. Persram and C. Gale, Phys. Rev. C **65**, 064611 (2002).

[12] B.-A. Li and L.-W. Chen, Phys. Rev. C **72**, 064611 (2005).
[13] Cai Xiangzhou, Feng Jun, Shen Wenqing, Ma Yugang, Wang Jiansong, and Ye Wei, Phys. Rev. C **58**, 572 (1998).
[14] G. Q. Li and R. Machleidt, Phys. Rev. C **48**, 1702 (1993); **49**, 566 (1994).
[15] H.-J. Schulze, A. Schnell, G. Röpke, and U. Lombardo, Phys. Rev. C **55**, 3006 (1997).
[16] F. Sammarruca and P. Krastev, Phys. Rev. C **73**, 014001 (2006).
[17] R. Machleidt, Adv. Nucl. Phys. **19**, 189 (1989).
[18] R. Machleidt, Phys. Rev. C **63**, 024001 (2001).
[19] V. G. J. Stoks, R. A. M. Klomp, C. P. F. Terheggen, and J. J. deSwart, Phys. Rev. C **49**, 2950 (1994).
[20] R. H. Thompson, Phys. Rev. D **1**, 110 (1970).
[21] E. E. Salpeter and H. A. Bethe, Phys. Rev. **84**, 1232 (1951).
[22] F. Sammarruca, Int. J. Mod. Phys. E **19**, 1259 (2010).
[23] L. C. Gomes, J. D. Walecka, and V. F. Weisskopf, Ann. Phys. (NY) **3**, 241 (1958).
[24] M. S. Hussein, R. A. Rego, and C. A. Bertulani, Phys. Rep. **201**, 279 (1991).
[25] C. A. Bertulani, Braz. J. Phys. **16**, 380 (1986).
[26] C. A. Bertulani, J. Phys. G **27**, L67 (2001).